Journal of Sound and Vibration (1999) **225**(3), 581–594
Article No. jsvi.1999.2176, available online at http://www.idealibrary.com on IDEAL®

SHEAR DEFORMATION CORRECTION TO TRANSVERSE SHAPE RECONSTRUCTION FROM DISTRIBUTED STRAIN MEASUREMENTS

M. D. TODD AND S. T. VOHRA

Optical Sciences Division, Naval Research Laboratory, Washington, DC 20375, *U.S.A.*

(*Received* 11 *February* 1999)

1. INTRODUCTION

Significant recent attention has been given to the assessment of the nation's rapidly aging infrastructure. For example, 50% of the National Highway System's 260,000 km of roadway has been rated as "poor to fair" [1], and about 32% of 576,000 bridges in service have been rated as "deficient" [2]. Such studies have fostered efforts in populating civil structures such as bridges with sensor arrays [3, 4] whose measurements are able to be analyzed with an eye towards condition assessment and/or damage detection [5–7]. These data could be aggregately incorporated into databases that may become useful in predicting or re-evaluating service life.

Traditional sensing strategies have focused primarily on conventional distributed strain measurement networks, where typically on the order of only 10–25 independent sensors are used due to hardware limitations, cost, or both [8]; this relative paucity of data points can be insufficient for proper dynamic interrogation of a structure such as a bridge. However, the emergence and maturity of fiber Bragg grating (FBG) optical strain-sensing systems has provided a useful alternative, offering advantages of electromagnetic immunity, negligible invasiveness, corrosion resistance, and structural-grade performance with inherent multiplexibility [9]. Their wavelength-encoded operation principle, along with appropriate demultiplexing electronics technology, have made high sensor count FBG arrays a practical tool in bridge monitoring [10].

With such hardware in place for adequate strain data collection, it is often important, especially when considering the inputs needed for various condition assessment or damage detection algorithms, to measure the dynamic deflection of the bridge. A number of axial strain-to-displacement methods have been demonstrated including global basis functions [11, 12], local basis functions [13–15], and methods utilizing modal test data [16]. The basis function methods involve choosing *a priori* a set of functions in the axial co-ordinate which are fit to measured strain data over some known length of the structure and implementing a simplified formulation of the Cauchy tensor which relates strain to displacement, e.g., the Euler–Bernoulli theory. In the case of global functions, this operation is completed over relatively large length scales of the structure, e.g., an entire span of

0022-460X/99/330581 + 14 $30.00/0

a bridge, while with local functions, the structure is discretized into elements, and the strain is usually assumed to be a quadratic polynomial. The overall deflection of the structure is constructed piece-wise by enforcing continuity of deflection and slope between elements.

The common relationship invoked in all of these basis function methods, at least when the structure is assumed to be primarily one-dimensional (such as with a bridge), is the Euler–Bernoulli beam theory. This well-known classic theory, which assumes that plane sections normal to the beam's centroidal axis remain normal under bending, has been shown to be a very useful and easily implemented theory for a number of long, slender structures where the radius of gyration is negligible compared to the axial length. One implication of this theory is the neglect to shear strain and for cases where the shear strain is not negligible, Timoshenko formulated a theory, e.g., see reference [17], whereby deformation is coupled to both bending and shearing effects. While many bridges have long spans and relatively shallow supporting girders—a situation for which Euler–Bernoulli theory is likely appropriate—many short-span overpass bridges or railway bridges (with very deep supporting girders) may violate negligible radius of gyration assumptions and require a shear correction.

This paper will present a global basis functional method in which shear effects are included but no independent measurements of the shear strain are needed to reconstruct the transverse displacement. The resulting strain-to-displacement relationship, like with the Euler–Bernoulli formulation, is suitable for application of a global basis function approach. After presenting the method, this paper will demonstrate it utility on two examples: (1) a statistically loaded multi-span beam, and (2) a single-span beam loaded with a moving concentrated load, serving as a crude model of a bridge span being traversed by a single vehicle. Although the example of bridges will be exploited in this paper, it is expected that this shear-corrected method will provide, for *any* beam-like structure where slenderness assumptions are suspect, an improved deflection estimate from measured axial strain data.

2. THEORETICAL DEVELOPMENT

2.1. SHEAR DEFORMATION EFFECTS

When shear deformation is considered along with the usual pure bending effects in the transverse deflection of a beam, Timoshenko theory [17] states that

$$\frac{\partial w(x,t)}{\partial x} = \Psi(x,t) + \beta(x,t), \tag{1}$$

where $w(x,t)$ is the transverse deflection, $\Psi(x,t)$ is the rotation of normal lines to the beam's centroidal axis (centerline) under bending deformation, and $\beta(x,t)$ is the rotation of tangent lines to the beam's centerline under shearing deformation. The contribution of $\Psi(x,t)$ is shown in Figure 1(a); segment m–n maps to segment m'–n' under pure bending. Conversely, in Figure 1(b), with consideration of shear effects only, segment m–n remains the same, while segment a–b maps to segment a–b'.

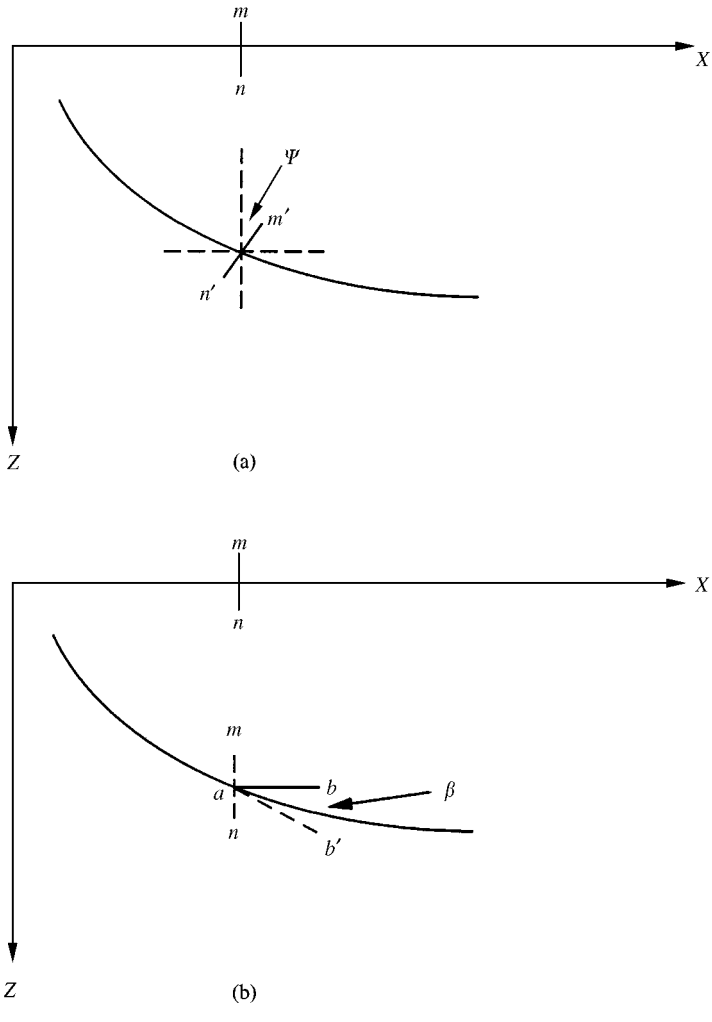

Figure 1. (a) A beam section subject to pure bending; (b) a beam section subject to pure shear deformation.

Hence, these two effects, under the linearization associated with small deflections, can be superimposed as in equation (1).

One implied assumption in equation (1) is that the angle β is constant in z, which means the shear strain (stress) is constant over the beam thickness. While this cannot occur under transverse normal loading, functional dependence upon z removes the inherent simplicity of one-dimensional beam theory, and the discrepancy can be reasonably remedied with the application of a shear correction factor, k_s [18].

The total displacement vector $\hat{\mathbf{u}}$ in the x and z directions of a point along the centerline is $\hat{\mathbf{u}} = u(x, z, t)\hat{\mathbf{i}} + w(x, t)\hat{\mathbf{k}}$, where the horizontal displacement component $u(x, z, t)$ for a point at a distance z away from the centerline is $u(x, z, t) = -z\Psi(x, t)$. From the linearized strain-displacement components of the

Cauchy tensor

$$\varepsilon_{ij} = \tfrac{1}{2}(u_{i,j} + u_{j,i}), \tag{2}$$

the two non-zero strains for a one-dimensional beam structure are given by

$$\varepsilon_{xx} \equiv \varepsilon = \frac{1}{2}\left(\frac{\partial u}{\partial x} + \frac{\partial u}{\partial x}\right) = -z\frac{\partial \Psi}{\partial x}, \tag{3}$$

$$\varepsilon_{xz} \equiv \gamma = \frac{1}{2}\left(\frac{\partial u}{\partial z} + \frac{\partial w}{\partial x}\right) = \frac{1}{2}\beta, \tag{4}$$

where no purely axial loads have been applied, and equation (1) has been used in equation (4).

Minimization of the Lagrangian, with shear deformation effects included, yields the governing equations for an isotropic beam:

$$-EI\frac{\partial^2 \Psi}{\partial x^2} + k_s GA\left(\Psi - \frac{\partial w}{\partial x}\right) = 0,$$

$$\rho A\frac{\partial^2 w}{\partial t^2} + k_s GA\left(\frac{\partial \Psi}{\partial x} - \frac{\partial^2 w}{\partial x^2}\right) = q(x, t), \tag{5}$$

where E is Young's modulus, $G = E/2(1 + v)$ is the shear modulus, I is the area moment of inertia, A is the cross-sectional area, v is the Poisson ratio, and $q(x, t)$ is the applied distributed transverse load. Decoupling these equations and non-dimensionalizing results in the equation for the deflection $w(x, t)$,

$$\mu^2\frac{\partial^4 w}{\partial x^4} - r^2(1 + \kappa^2)\frac{\partial^4 w}{\partial x^2 \partial t^2} + \frac{\partial^2 w}{\partial t^2} = \mu^2 Q - r^2\kappa^2\mu^2\frac{\partial^2 Q}{\partial x^2}, \tag{6}$$

where $x = x/L$, $w(x, t) = w(x, t)/L$, $r^2 = I/AL^2$, $\mu^2 = EI/\rho AL^4$, $\kappa^2 = 2(1 + v)/k_s$, and $Q(x, t)$ is the non-dimensionalized transverse load. Euler–Bernoulli theory assumes that r is small compared to unity and can be neglected, which would result in the familiar classical expression

$$\mu^2\frac{\partial^4 w}{\partial x^4} + \frac{\partial^2 w}{\partial t^2} = \mu^2 Q. \tag{7}$$

This is usually an accurate assumption for slender beam structures which have a long length compared to thickness, as r typically varies as the ratio of thickness to length.

2.2. TRANSVERSE SHAPE RECONSTRUCTION

As discussed previously, shape reconstruction approaches typically have ignored shear deformation effects, primarily because the resulting Euler–Bernoulli strain–displacement relationship is very tractable. If shear strain γ is neglected, then

$\Psi = \partial w/\partial x$, and equation (3) becomes, after rearranging,

$$\frac{\partial^2 w}{\partial x^2} = -\left(\frac{1}{z}\right)\varepsilon. \tag{8}$$

At this point, a set of basis functions is chosen to fit measured strain values, and the constructed strain function is integrated twice with respect to x in accordance with equation (8) with appropriate uniqueness or boundary conditions to approximate the deflection $w(x, t)$. Strictly speaking, in the cases of dynamic behavior, this reconstruction approach would have to be preformed at each time step in order to recover successfully the time history of the deflection.

If shear deformation effects are not neglected, however, it may appear that the coupled nature of the governing equations (5) and the strain–displacement relationships of equations (3) and (4) would require measurement of both axial and shear strains independently in order to reconstruct $w(x, t)$. However, if equation (1) is differentiated with respect to x, and equations (3) and (4) are utilized, the result is

$$-\left(\frac{1}{z}\right)\varepsilon = \frac{\partial^2 w}{\partial x^2} - 2\frac{\partial \gamma}{\partial x}. \tag{9}$$

Similarly, substitution of equations (3) and (4) into the first of equations (5) yields

$$EI\left(\frac{1}{z}\right)\frac{\partial \varepsilon}{\partial x} - 2k_s GA\gamma = 0. \tag{10}$$

The strains in equations (9) and (10) can then be decoupled to give, after rearranging,

$$\frac{\partial^2 w}{\partial x^2} = -\left(\frac{L}{z}\right)\left(\varepsilon - r^2\kappa^2\frac{\partial^2 \varepsilon}{\partial x^2}\right), \tag{11}$$

where the same parameter substitutions and non-dimensionalizations made in equation (6) were made here. This equation directly relates the shear-corrected transverse deflection $w(x, t)$ to the axial strain ε only, thus requiring no independent measurements of shear strain γ. Again, allowing $r \to 0$ recovers the Euler–Bernoulli formulation, (8).

It is assumed, as before, that the strain ε at each instant of time t can be represented as a sum of general global basis functions $\phi_i(x)$, or

$$\varepsilon = \sum_{i=0}^{N-1} a_i \phi_i(x), \tag{12}$$

where the a_i are unknown coefficients (dependent on the current time step if dynamics are involved), and N is less than or equal to the number of total strain measurements made. The choice of basis functions is somewhat arbitrary, provided they are smoothly differentiable; logical choices for $\phi_i(x)$ include the dynamic mode shapes and polynomials, typically depending upon what types of loading are expected. If the strain measurements are obtained with sensors whose gage lengths are non-negligible relative to the axial length of the structure, an average strain $\bar{\varepsilon}$ is measured at their locations. In terms of the assumed basis function expansion, the

average strain $\bar{\varepsilon}_j$ measured at the jth sensor location is

$$\bar{\varepsilon}_j = \left(\frac{1}{\beta_j - \alpha_j}\right) \int_{\alpha_j}^{\beta_j} \varepsilon \, \mathrm{d}x = \left(\frac{1}{\beta_j - \alpha_j}\right) \sum_{i=0}^{N-1} \int_{\alpha_j}^{\beta_j} a_i \phi_i(x) \, \mathrm{d}x = \sum_{i=0}^{N-1} a_i c_{ji}, \tag{13}$$

where $|\beta_j - \alpha_j|$ is the gage length of the jth sensor, and c_{ji} is the average value of ϕ_i over $[\alpha_j \leqslant x \leqslant \beta_j]$. Since at least N of these measurements have been obtained, and there are N of the unknown a_i, a linear system in the a_i is defined by the last of equations (13). This system is well conditioned and directly invertible if N equals the number of measurements taken, or $a_i = c_{ji}^{-1} \bar{\varepsilon}_j$. If N is less than the number of measurements taken, equation (13) can be solved in a least-squares sense. If the sensor gage length is negligible in relation to the structure size, i.e., $\beta_j \to \alpha_j$, then $c_{ji} \to \phi_i(\alpha_j)$.

The instantaneous deflection $w(x) \equiv w(x, t)$ can thus be represented, using equations (11) and (12) and rearranging,

$$w(x) = -\frac{1}{z} \sum_{i=0}^{N-1} a_i [\Phi_i(x) - \kappa^2 r^2 \phi_i(x)] + c_1 x + c_2, \tag{14}$$

where $\Phi_i(x)$ is the indefinite double integral of $\phi_i(x)$ with respect to x, the constants c_1 and c_2 arise from the indefinite integration, and the a_i are now presumed known from the inversion of or the least-squares solution of equation (13). The constants can be obtained by specifying two boundary conditions for the beam; typically, these displacements are zero, and using $w(0) = w(1) = 0$,

$$\begin{aligned} c_1 &= \frac{L}{z} \sum_{i=0}^{N-1} a_i (\Phi_i(1) - \Phi_i(0) - \kappa^2 r^2 (\phi_i(1) - \phi_i(0))), \\ c_2 &= \frac{L}{z} \sum_{i=0}^{N-1} a_i (\Phi_i(0) - \kappa^2 r^2 \phi_i(0)). \end{aligned} \tag{15}$$

Equation (14) applies to a single beam and can be extended to a structure that is composed of a number of connected beam elements, e.g., as in a bridge where each span between supports could be thought of as "beam". Each span can be described by a function similar to equation (14) with the added conditions of continuous slope and deflection across spans to retain solution uniqueness.

3. SHAPE RECONSTRUCTION EXAMPLES

3.1. STATIC LOAD

As a first example, we consider a two-span beam statistically loaded with the load distribution as shown in Figure 2(a), The static solution $[w(x), \Psi(x)]$ of the coupled equations (5) with simply supported boundary conditions at each end and continuity of slope and deflection cross the middle support was obtained, and the axial strain was computed by equation (3). This strain function was used to generate the measurement data at four suboptimized sensor locations along each span for a total of eight measurements.

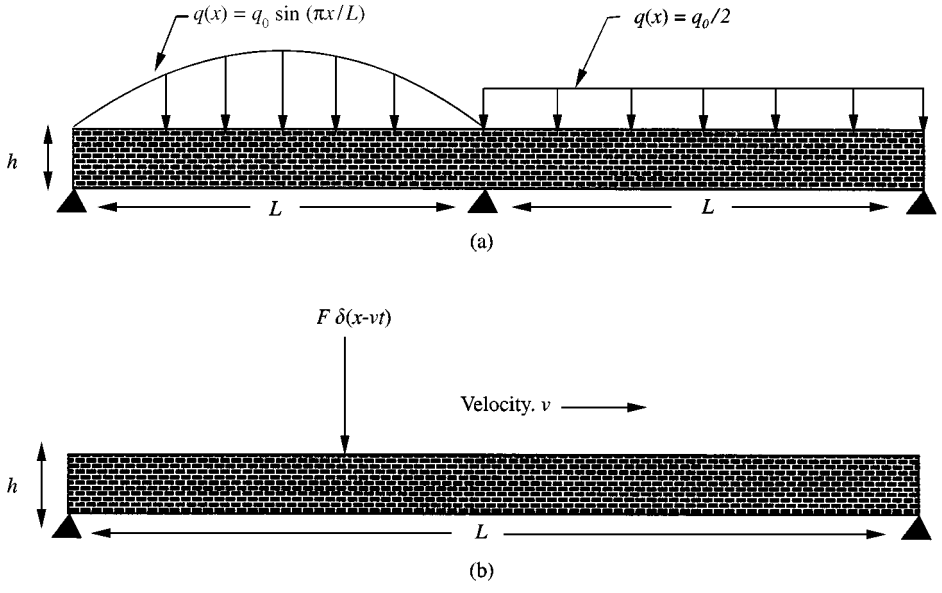

Figure 2. Load distribution for (a) static example; (b) dynamic example.

For shape reconstruction in this case, a polynomial function basis was chosen for $\phi_i(x)$, resulting in a cubic polynomial (four unknown coefficient associated with four measurements) for strain and a quintic polynomial for displacement. Polynomials were chosen because they form a natural basis in statically loaded beam problems. Gage lengths were assumed to be negligible such that $c_{ji} = \alpha_j^i$, and the results comparing the estimated shape to the exact analytical shape are shown in Figure 3 for various values of κr. Further comparison was drawn by including the shape reconstruction based on the Euler–Bernoulli approach. For small κr, i.e., for a small radius of gyration, the results all tend to match, as expected. As κr is increased, however, shear effects are no longer negligible, and a clear discrepancy is observed between the shear deformation formulation and the Euler–Bernoulli formulation. At $\kappa r = 0{\cdot}25$, the Euler–Bernoulli shape estimation appears to deviate significantly from the exact shape, while the shear-corrected estimation continues to approximate the shape well.

A more quantitative measure of the error associated with the shape estimation can be obtained by defining the root-mean-square error σ of the difference between the basis fit and the exact shape function

$$\sigma = \sqrt{\frac{1}{L}\int_0^L (w(x) - \hat{w}(x))^2 \, \mathrm{d}x}, \tag{16}$$

where $w(x)$ is the exact deflection, and $\hat{w}(x)$ is the reconstructed deflection using the chosen function basis. For the example under current consideration, this integral was calculated for both the shear-connected expression [equation (11)] and the Euler–Bernoulli expression [equation (8)] using the polynomial basis. The results are shown in Table 1 for three different values of κr and three different

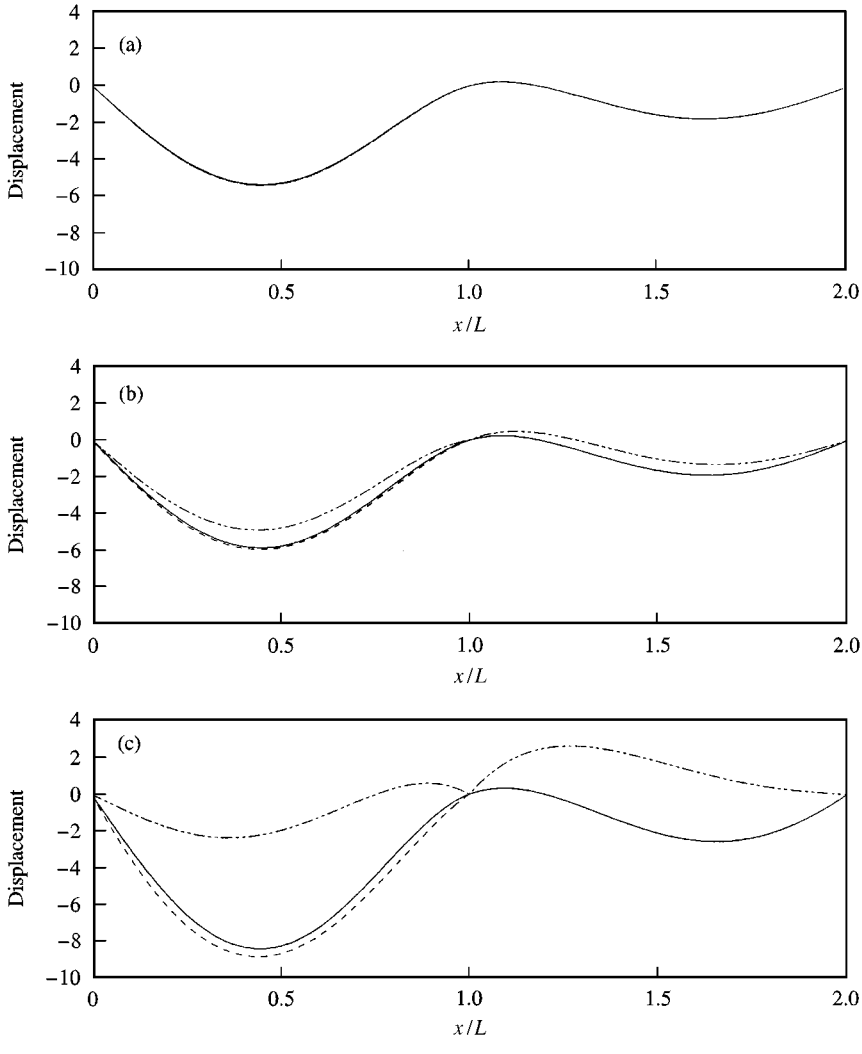

Figure 3. Exact and estimated displacements with $\delta = 0$ for (a) $\kappa r = 0$, (b) $\kappa r = 0{\cdot}1$, (c) $\kappa r = 0{\cdot}25$; 4 sensors/span were used; —, exact; ---, shear corrected; – · · –, Euler-Bernoulli.

TABLE 1

A comparison of error between shear-corrected and Euler–Bernoulli formulations for the shape estimtion of a two-span statistically loaded beam: variable sensor count, no added noise

	$\sigma_{\text{shear-corrected}}$			$\sigma_{\text{Euler-Bernoulli}}$		
	$\mu = 0{\cdot}0$	$\mu = 0{\cdot}1$	$\mu = 0{\cdot}5$	$\mu = 0{\cdot}0$	$\mu = 0{\cdot}1$	$\mu = 0{\cdot}5$
3 sensors/span	$8{\cdot}73 \times 10^{-5}$	$1{\cdot}79 \times 10^{-4}$	$2{\cdot}27 \times 10^{-3}$	$8{\cdot}73 \times 10^{-5}$	$3{\cdot}88 \times 10^{-3}$	$3{\cdot}17 \times 10^{0}$
4 sensors/span	$2{\cdot}38 \times 10^{-5}$	$9{\cdot}87 \times 10^{-5}$	$1{\cdot}91 \times 10^{-3}$	$2{\cdot}38 \times 10^{-5}$	$6{\cdot}94 \times 10^{-4}$	$1{\cdot}79 \times 10^{-2}$
5 sensors/span	$1{\cdot}90 \times 10^{-7}$	$5{\cdot}81 \times 10^{-6}$	$1{\cdot}43 \times 10^{-4}$	$1{\cdot}90 \times 10^{-7}$	$7{\cdot}17 \times 10^{-4}$	$1{\cdot}79 \times 10^{-2}$

TABLE 2

A comparison of error between shear-corrected and Euler–Bernoulli formulations for the shape estimtion of a two-span statistically loaded beam: 5 sensors/span, variable noise

	$\sigma_{\text{shear-corrected}}$			$\sigma_{\text{Euler-Bernoulli}}$		
	$\mu = 0{\cdot}0$	$\mu = 0{\cdot}1$	$\mu = 0{\cdot}5$	$\mu = 0{\cdot}0$	$\mu = 0{\cdot}1$	$\mu = 0{\cdot}5$
$\delta = 0{\cdot}01$	$7{\cdot}68 \times 10^{-5}$	$1{\cdot}85 \times 10^{-4}$	$4{\cdot}71 \times 10^{-3}$	$7{\cdot}68 \times 10^{-5}$	$7{\cdot}65 \times 10^{-4}$	$1{\cdot}80 \times 10^{-2}$
$\delta = 0{\cdot}04$	$5{\cdot}72 \times 10^{-4}$	$1{\cdot}24 \times 10^{-3}$	$1{\cdot}81 \times 10^{-2}$	$5{\cdot}72 \times 10^{-4}$	$1{\cdot}55 \times 10^{-2}$	$3{\cdot}39 \times 10^{0}$

sensor counts for each span. Provided $\kappa r \neq 0$, the error calculated in the shear-corrected formulation is always smaller, with equivalence at $\kappa r = 0$, as expected; in many cases, the error is as much as two orders of magnitude less. Furthermore, the error decreases with increased sensor count, also as expected. It should be reiterated that the sensor locations were not optimized in any way such that absolute values of σ are not as globally meaningful as relative values; it is possible that *all* the values presented in Table 1 can be reduced, perhaps even significantly, merely by judicious sensor placement [19].

In any real measurement, a certain amount of error also arises, not due to model short-comings or even sensor density and placement issues, but rather due to inherent performance characteristics of the measurement device. To simulate this effect, a random noise component with zero mean and a range of $\pm \delta(q_0 z L^2/EI)$ was added to the strain measurements. Using a constant five sensors/span, the values of σ were obtained as shown in Table 2. Increases in δ degraded the estimation algorithms, although the shear-corrected formulation remained more robust. The visual effects of the noise on the estimated shapes are shown in Figures 4 and 5. For $\delta = 0{\cdot}01$, the effects of sensor noise do not appear significant until $\kappa r = 0{\cdot}25$, especially when compared to Figure 3. For $\delta = 0{\cdot}04$, the error, particularly in the Euler–Bernoulli formulation, becomes considerable, and even the shear formulation miscalculates the shape. It can be shown that as $\delta \to \kappa^2 r^2$, sensor noise influences can become significant enough to negate any advantage gained by including the shear correction terms. For fiber optic strain-sensing systems, where nanostrain resolution is possible, this condition is unlikely to be met unless very small loads relative to the structure's inherent bending characteristics are present.

3.2. DYNAMIC LOAD

For a dynamically loaded example, we consider Figure 2(b), where a single-span simply supported beam is excited by a point load moving from left to right across the beam at velocity v (chosen to be 0·1 in the forthcoming example, which is well below the first resonance of the span). Such an example could approximately model

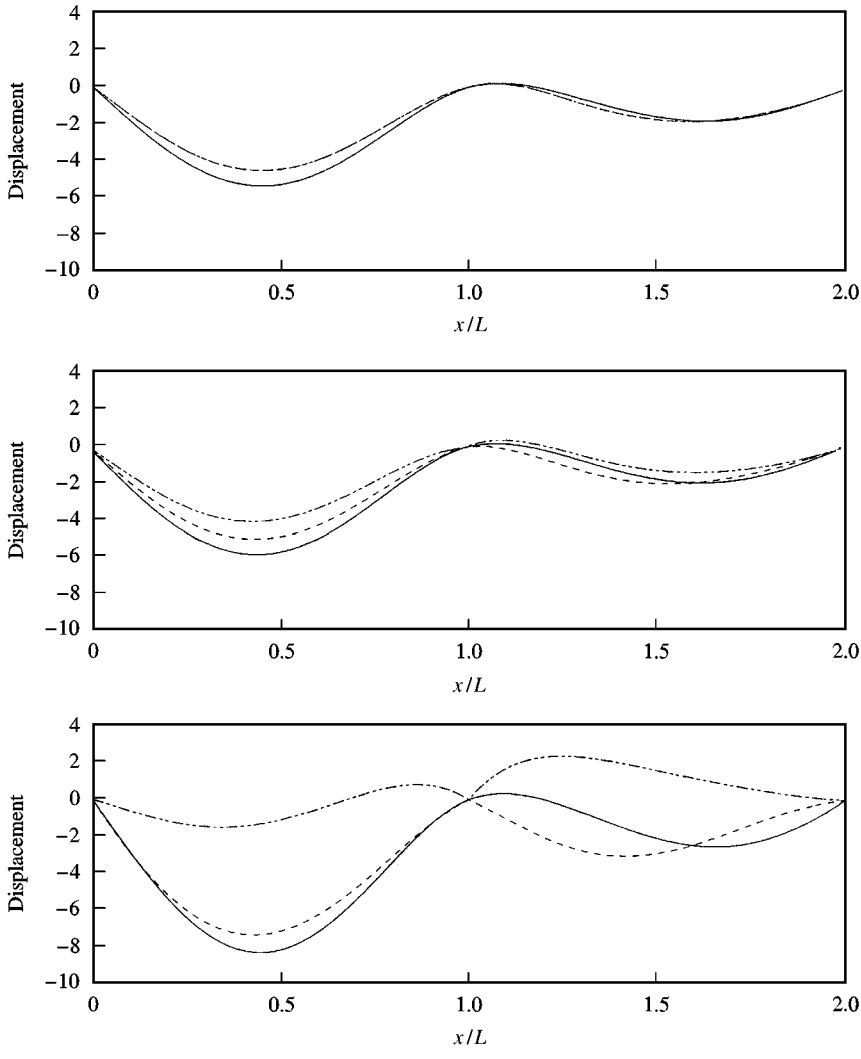

Figure 4. Exact and estimated displacements with $\delta = 0{\cdot}01$ for (a) $\kappa r = 0$, (b) $\kappa r = 0{\cdot}1$, (c) $\kappa r = 0{\cdot}25$; 4 sensors/span were used; —, exact; ---, shear corrected; – · · –, Euler-Bernoulli.

a vehicle moving across a bridge span. The full-coupled equations (5) were solved using modal superposition, where the eigenmodes chosen for $w(x, t)$ and $\Psi(x, t)$ were those for a simply supported Euler–Bernoulli beam. The axial strain at any time t was again computed from equation (3). For basis functions, the simply supported eigenmodes were also used, with sensor gage lengths again assumed negligible.

Figure 6 compares the exact, shear-corrected, and Euler–Bernoulli results at $t = 0{\cdot}08$ s, just as the point load moves on to the span, for different values of κr. Eight sensors evenly distributed across the span were used to reconstruct the deflections, and 16 modes were chosen to construct the exact solution. As in the static case, very small values of κr do not discriminate greatly between approaches.

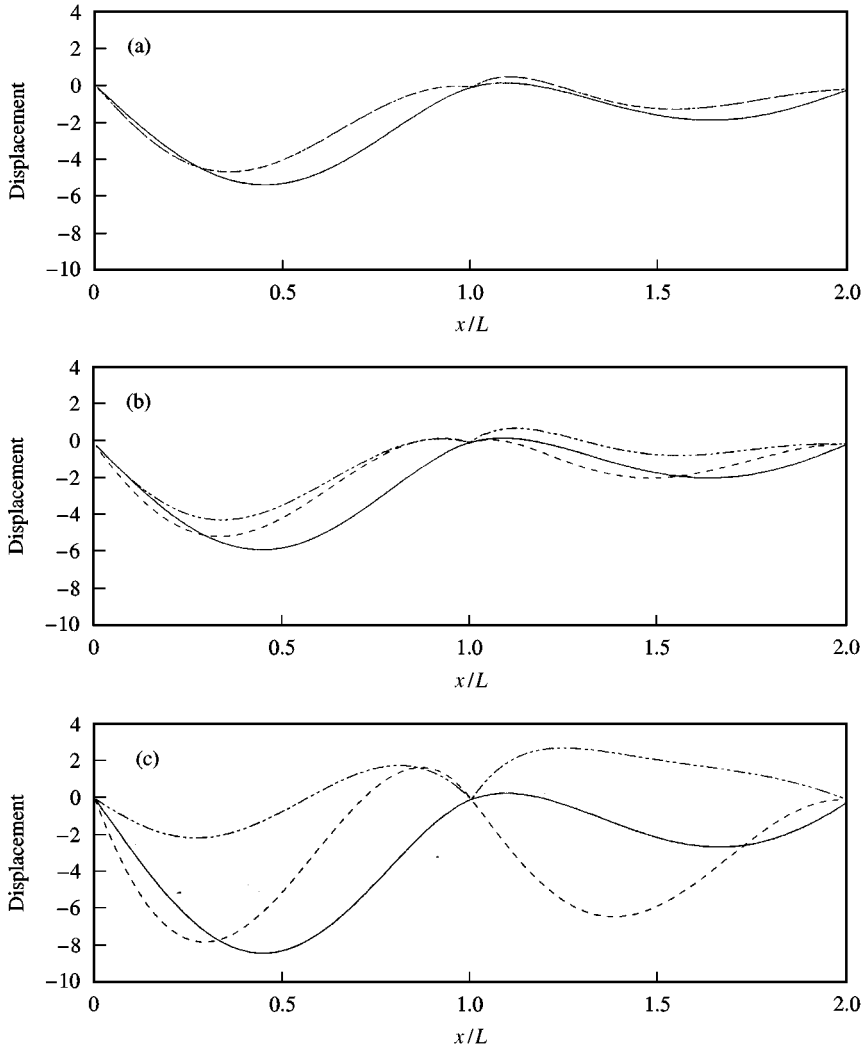

Figure 5. Exact and estimated displacements with $\delta = 0{\cdot}04$ for (a) $\kappa r = 0$, (b) $\kappa r = 0{\cdot}1$, (c) $\kappa r = 0{\cdot}25$; 4 sensors/span were used; —, exact; ---, shear corrected; – · · –, Euler-Bernoulli.

However, at $\kappa r = 0{\cdot}25$, only the shear-corrected approach captures any of the poly-modal behavior at that instant; the Euler–Bernoulli reconstruction is not only qualitatively misrepresentative but also quantitatively incorrect by an order of magnitude. However, even when a relatively large number of modes are not acting, the Euler–Bernoulli formulation fails at higher κr. Figure 7 compares the same data as Figure 6 at $t = 0{\cdot}5$ s, just as the point load is moving past mid-span, and the span is nearly undergoing its maximum deflection. The shear-corrected formulation, in this case, almost exactly reproduces the exact shape, while the Euler–Bernoulli formulation is off by almost 50%. Such an error could have serious consequences on estimating load, bending moment or shear force, and modal participation levels.

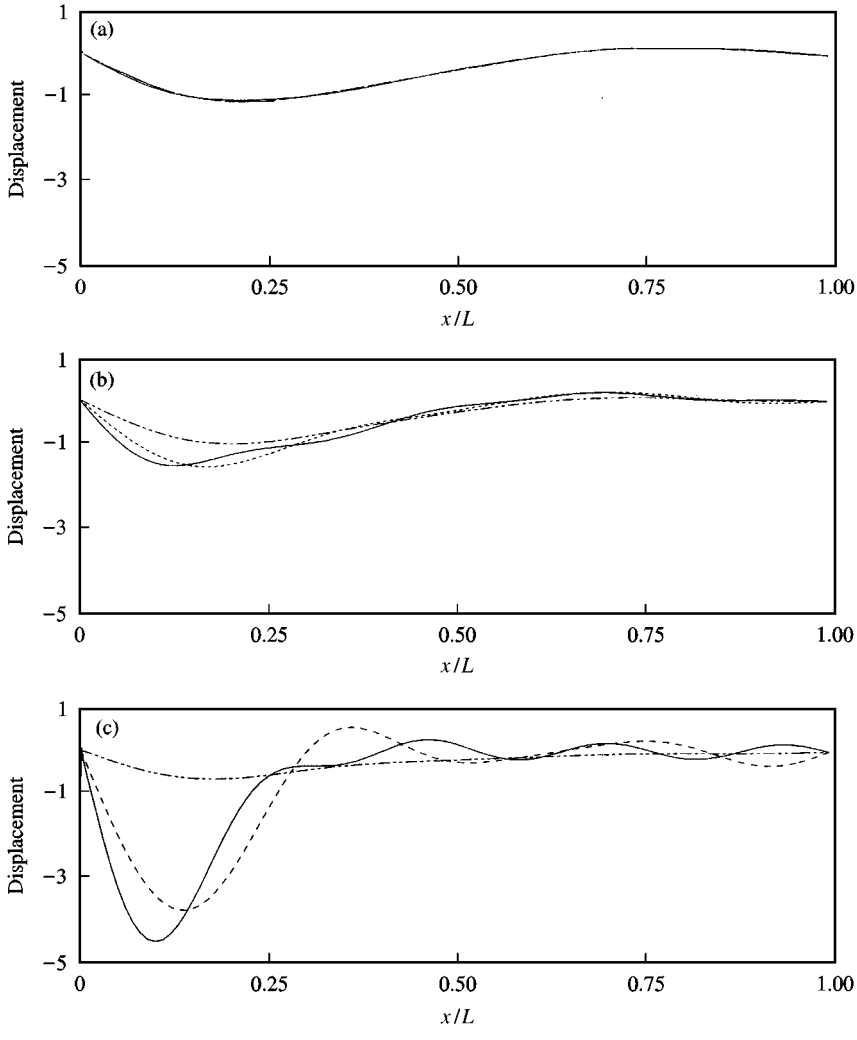

Figure 6. Exact and estimated dynamic displacements at $t = 0{\cdot}08$ for (a) $\kappa r = 0$, (b) $\kappa r = 0{\cdot}1$, (c) $\kappa r = 0{\cdot}25$; 8 sensors were used; —, exact; ---, shear corrected; – · · –, Euler-Bernoulli.

4. SUMMARY

This paper has developed a shear-corrected extension, making use of Timoshenko beam theory, of global basis function approaches to shape reconstruction of one-dimensional structures from axial strain measurements. The method accurately accounts for shear deformation effects, typically most prevalent in structures with non-negligible rotary inertia compared to length, without the necessity of independently measuring shear strain directly; this is an important consideration from the viewpoint of sensor count and placement optimization. Such formulation can be readily applied in real time, depending upon the measurement acquisition rate and the number of sensors, as processor time will be distributed between inverting the matrix c_{ji} at each time step (assuming a dynamic

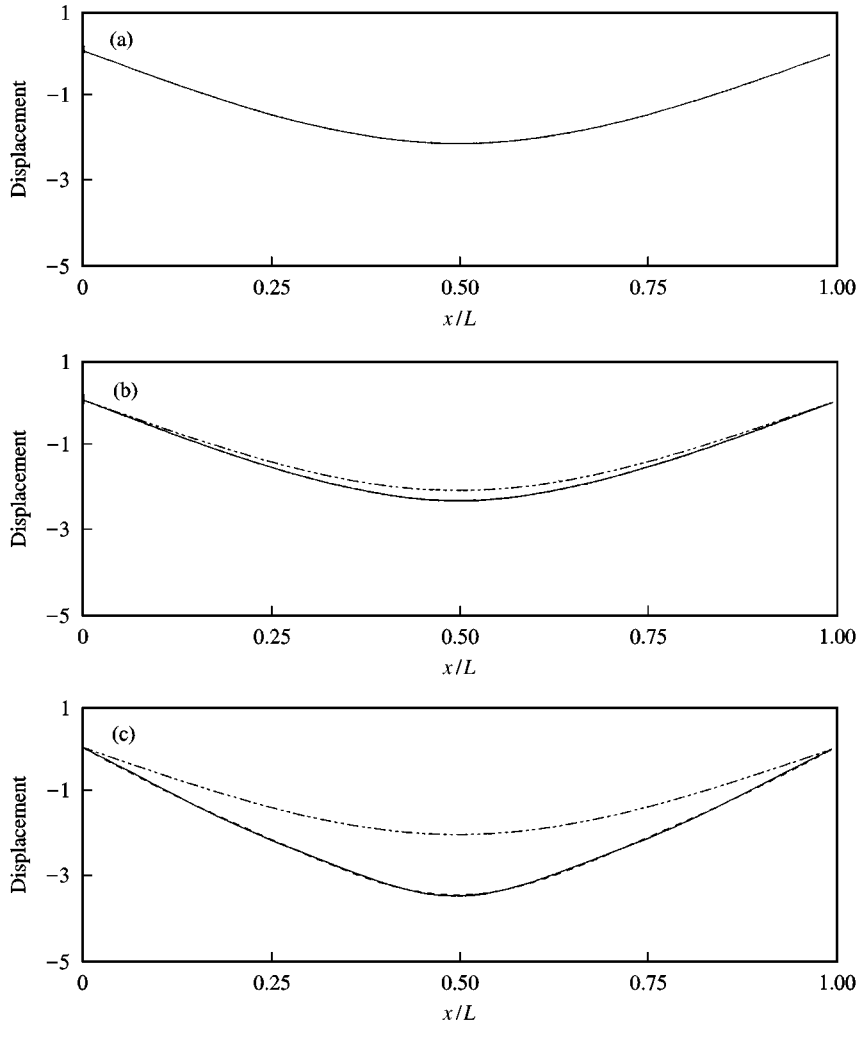

Figure 7. Exact and estimated dynamic displacements at $t = 5$ for (a) $\kappa r = 0$, (b) $\kappa r = 0{\cdot}1$, (c) $\kappa r = 0{\cdot}25$; 8 sensors were used; —, exact; ---, shear corrected; – · · –, Euler-Bernoulli.

load) and sampling the next data point. While the specific structural context of this paper was bridges, it is expected that this formulation can be used on any pseudo-one dimensional structure where axial strain measurements are readily obtained, such as ship hull sub-structures, truss configurations, or stiffening elements on larger structures. Data from such sensor-populated structures, used in conjunction with analysis such as shape reconstruction, can provide an important component in building a structural health monitoring system.

REFERENCES

1. U. D. Of Transportation 1995 *Technical Report FHWA-PL-96-007*, status of the nation's surface transportation system: condition and performance.

2. S. B. Chase and G. L. Washer 1997 *Public Roads* **61**, 16–25. Nondestructive evaluation for bridge management in the next century.
3. D. R. Huston and P. L. Fuhr 1998 *Fiber Optic Sensors for Construction Materials and Bridges*, Technomic Distributed and chemical fiber optic sensing and installation in bridges.
4. R. Maaskant, T. Alavie, R. M. Measures, G. Tadros, S. H. Rizkalla and A. Guha-Thakurta 1996 *Cement and Concrete Composites* **19**, 21–23. Fiber-optic Bragg grating sensors for bridge monitoring.
5. D. F. Mazurek, S. R. Jordan, D. J. Palazzetti and G. S. Robertson 1992 *Proceedings of the Nondestructive Evaluation of Civil Structures and Materials*. Damage detectability in bridge structures by vibrational analysis.
6. J. T. DeWolf, P. E. Coon and P. N. O'Leary 1995 *Extending the Lifespan of Structures, IABSE Vol.* 73/2, International Association for Bridge and Structural Engineering, 935–940. Continuous monitoring of bridge structures.
7. A. E. Atkan, V. Dalal, A. Helmicki, V. Hunt, M. Lennett, N. Catbas and A. Levi 1996 *Proceedings of the third Conference Nondestructive Evaluation of Civil Structures and Materials*. Objective bridge condition assessment for serviceability.
8. R. A. Livingston 1998 *Fiber Optic Sensors for Construction Materials and Bridges, Technomic*, 148. Federal highways administration research program in fiber optics for the infrastructure.
9. A. D. Kersey, M. A. Davis, H. J. Patrick, M. LeBlanc, K. P. Koo, C. G. Askins, M. A. Putnam and E. J. Friebele 1997 *Journal Lightwave Technology* **15**, 1442–1463. Fiber grating sensors.
10. S. T. Vohra, C. C. Chang, B. A. Danver, B. Althouse, M. A. Davis and R. Idriss 1998 *Fiber Optic Sensors for Construction Materials and Bridges, Technomic*. Preliminary results on the monitoring of an in-service bridge using a 32-channel fiber Bragg grating sensor system.
11. M. A. Davis, A. D. Kersey, J. Sirkis and E. J. Friebele 1994 *SPIE 2191*, 94–101. Fiber optic bragg grating array for shape and vibration mode shape sensing.
12. M. D. Todd, C. C. Chang, G. A. Johnson, S. T. Vohra, J. W. Pate and R. L. Idriss 1999 *IMAC XVII Applied Modal Analysis, SEM*, Bridge monitoring using a 64-channel fiber Brgg grating system.
13. M. Gopinathan, G. A. Pajunen, P. S. Nellakanta and M. Arockasiamy, 1995 *Journal of Intelligent Material Systems and Structures* **6**, 537–549. Recursive estimation of displacement and velocity in a cantilever beam using a measured set of distributed strain data.
14. S. Vurpillot, D. Inaudi and A. Scano 1996 *Smart Systems for Bridges, Structures, and Highways, SPIE 3043*. Mathematical model for the determination of vertical displacement from internal horizontal measurements of a bridge.
15. G. C. Kirby, T. W. Lim, R. Weber, A. B. Bosse, C. Povich and S. Fisher 1997 SPIE *3041*, 72–81. Strain-based shape estimation algorithms for a cantilever beam.
16. G. C. Foss and E. D. Haugse 1995 *Proceedings of the 13th International Modal Analysis Conference*, 112–118. Using modal test results to develop strain to displacement transformations.
17. S. Timoshenko and J. N. Goodier 1951 *Theory of Elasticity* New York: McGraw-Hill.
18. G. R. Cowper 1966 *Journal of Applied Mechanics* **33**, 335–340. The shear coefficient in Timoshenko's beam theory.
19. M. Papadopoulos and E. Garcia 1998, *AIAA Journal* **36**, 256–263. Sensor placement methodologies for dynamic testing.